Chapter

Femtosecond Stimulated Raman Microscopy in C–H Region of Raman Spectra of Biomolecules and Its Extension to Silent and Fingerprint Regions

Rajeev Ranjan, Maria Antonietta Ferrara and Luigi Sirleto

Abstract

Stimulated Raman scattering (SRS) microscopy, based on vibrational spectroscopy, is able to perform *label-free* imaging with high sensitivity, high spatial and spectral resolution, 3D sectioning, and fast time of image acquisition, i.e., a few seconds. In this chapter, the implementation of a femtosecond SRS microscope, working in C–H or O–H region (>2800 cm^{-1}) of Raman spectra of biomolecules, is reported. Our microscope is realized by integration of a femtosecond (fs) SRS experimental setup with an inverted optical microscope equipped with fast mirror scanning unit. The microscope is provided with two femtosecond laser sources: a titanium-sapphire (Ti:Sa) laser oscillator and an optical parametric oscillator (OPO). In addition, the reliability of our system in C–H region is tested by localizations of lipid droplets inside adipocyte cells. Finally, the extension of microscope to silent region of <1800 cm^{-1} and fingerprint region of 1800–2800 cm^{-1} is also achieved by adding a second-harmonic generator to cascade the OPO and double its energy radiation. Definitely, our microscope is able to take on some recent challenges of SRS microscopy, including improvements of sensitivity and detection specificity.

Keywords: stimulated Raman scattering, optical imaging, nonlinear microscopy, label-free imaging, bio-imaging

1. Introduction

One of the most important subjects in life sciences is the noninvasive characterization of microscopic objects within a complex heterogeneous system by optical microscopy. Nowadays, fluorescence microscopy is the workhorse for cellular imaging. However, since most of small biomolecules, such as nucleosides, amino acids, fatty acids, choline, glucose, cholesterol, and small-molecule drugs, are intrinsically nonfluorescent, fluorescent tags are needed. Unluckily, these fluorescent probes, such as organic dyes, fluorescent proteins, or quantum dots, are all quite larger than small biomolecules; therefore they can severely falsify native biochemical or

biophysical properties of the observed biomolecules inside cells. Definitely, small biomolecules have a fundamental functional importance, but, unfortunately, are basically undetectable by fluorescence microscopy. Therefore, a label-free imaging, with high sensitivity, high spatial resolution, and high chemical selectivity of unlabeled living cells, is highly desirable [1, 2].

Among label-free techniques, exploiting nonlinear optical effects, stimulated Raman scattering (SRS) microscopy is one of the most promising techniques [3–12]. SRS, discovered in 1960 [13–15], is a third-order nonlinear process in which two collinear laser pulses are used as pump and probe (Stokes) beams at frequencies of ω_p and ω_s (while $\omega_p > \omega_S$) and are focused into the sample. When the energy difference between pump and probe beams is equivalent to a vibrational energy (ω_v) of the sample, an exchange of energy between the two beams occurs and results a gain in the Stokes signal (stimulated Raman gain, SRG) and a loss in the pump signal (stimulated Raman loss, SRL) [16–19], as shown in **Figure 1**. Experimentally, both the modalities of SRG and SRL can be detected.

Since the invention of the picosecond (ps) narrowband SRS microscopy, a variety of molecular species have been imaged by label-free SRS targeting their intrinsic chemical bonds at the crowded cellular fingerprint region of 500–1700 cm^{-1} or the high-frequency C–H or O–H region of 2800–3200 cm^{-1}. However, SRS microscopy has some limitations, too. Indeed, by considering that several biomolecular species share similar chemical bonds, in some cases, it could be difficult to separate a target biomolecule from all the other related species inside cells. This leads to a problematic detection specificity. Additionally, the endogenous chemical bonds have typically small Raman scattering cross sections. This limits the detection sensitivity

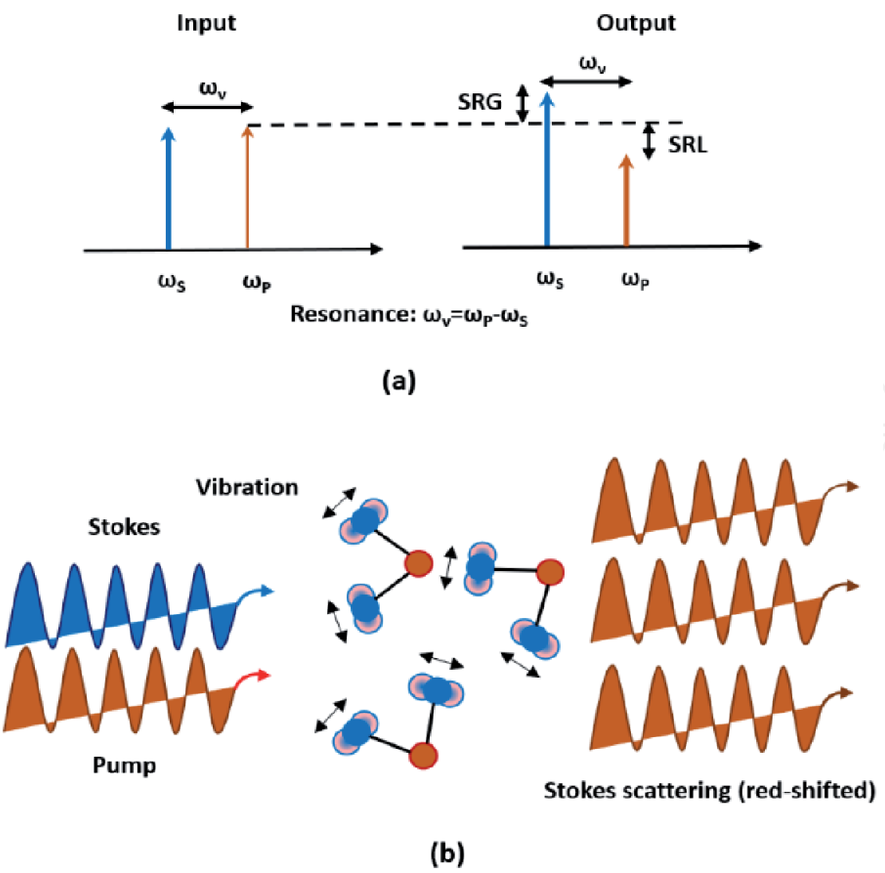

Figure 1.
SRS principle: (a) SRS modalities are described: SRG, stimulated Raman gain; SRL, stimulated Raman loss; and (b) stimulated Raman scattering occurs through the vibrationally excited molecules that interfere coherently.

of this approach to few millimolars, whereas a micromolar sensitivity is required for small biomolecules. Thus, there is a strong need to further increase specificity and sensitivity, as well as to probe dynamics [3–12].

Recently, to achieve detection specificity, general bio-orthogonal chemical imaging platform has emerged by coupling SRS microscopy with small Raman-active vibrational probes, such as alkynes and stable isotopes, which are both spectroscopically and biochemically orthogonal to the molecules inside cells, allowing a better sensitivity, specificity, and biocompatibility for imaging the small biomolecules. The improvement made by these vibrational probes is to shift Raman peaks in the cell-silent region where no other peaks from endogenous molecules are present [20–23].

Concerning SRS sensitivity, a 12 times larger stimulated Raman loss signal by femtosecond pulse excitation than picosecond pulse was demonstrated [24]. In literature, a number of interesting biological applications based on femtosecond SRS microscopy have been reported, extending to the silent region and encouraging the bio-orthogonal chemical imaging platform [25–30]. Definitely, femtosecond stimulated Raman microscopy and bio-orthogonal chemical appear as an unavoidable perspective for SRS improvements.

In multimodal imaging, single cells can be imaged in a single microscope by simultaneous image acquisition of various nonlinear imaging techniques: SRS, coherent anti-Stokes Raman scattering (CARS), second-harmonic generation (SHG), third-harmonic generation (THG), and sum frequency generation (SFG). The main advantages of multimodal imaging are that the same excitation source can be used for all imaging modalities, while generated signals by nonlinear interaction can be spectrally separated for simultaneous image collection in forward and/or backward detection, resolving structural diversity in biomaterials [31, 32].

In multimodal label-free microscopy, in order to take advantage of a single setup, several key laser parameters must be carefully considered. We note that SHG, THG, and multiphoton excitation fluorescence (MPEF) take advantage by short femtosecond pulses due to the nonlinear processes involved. For CARS and SRS, two synchronized pulses at the correct wavelength separation are required, so the laser system should have a wide spectral tunability in specific spectral regions. Therefore, in multimodal imaging to allow the most flexibility, the best choice are a femtosecond titanium-sapphire (Ti:Sa) oscillators and an optical parametric oscillator (OPO), where one of two laser beams can be used for single-beam techniques (SHG, THG, and MPEF), while their combination can be utilized for double-beam techniques (CARS or SRS) [31, 32].

However, although typical and widespread commercial laser sources, such as OPO pumped by Ti:Sa laser, are tailored for multimodal imaging, they present a limitation: Their minimum wavelength difference between pump (Ti:Sa laser) and signal (OPO) is 2500 cm^{-1}. Therefore, this laser combination allows only the CH-OH region exploration of Raman spectra, while the silent and fingerprint regions are out of the emission range [33–38]. As a consequence, this laser combination cannot accomplish the demand of bio-orthogonal platform based on femtosecond stimulated Raman microscopy, compromising its diffusion.

Recently, some new laser sources are available in the market. They allow to reach the silent region and fingerprint regions, but the pumping laser is a fiber one. It is well known that they have a relative intensity noise (RIN) greater than that of Ti:Sa laser oscillator, so a more complex detection system, for example, balanced detection, can be required. In this chapter in order to extend the potentiality of Ti:Sa laser and OPO combination and to avoid the drawback of fiber laser, an implementation of an SRS microscope is described, in which a third femtosecond source is added, i.e., a SHG cascading the OPO and doubling its energy radiation.

The chapter is organized as follows. In the next paragraph, the implementation and main realization issues of a femtosecond SRS microscope, working in C–H region, are illustrated. The microscope, equipped with two femtosecond laser sources, a Ti:Sa laser and an OPO output, covers the C–H region or O–H region (>2800 cm^{-1}) in stimulated Raman gain (SRG) modality. The successful implementation of our imaging system is demonstrated reporting label-free images of polystyrene beads with a diameter of 3 microns. In Subsection 2.1, SRS imaging is applied to investigate the distributions of lipid droplets (LDs) in 3T3-L1 cells at different stages of adipocyte differentiation process. In Section 3, the extension of previous SRS microscope to the silent and fingerprint regions, obtained by adding a third femtosecond laser source, i.e., a SHG cascading the OPO, is described. By combining the Ti:Sa laser and SHG output, the microscope covers not only the C–H region but also the fingerprint region (<1800 cm^{-1}) and the silent region (1800–2800 cm^{-1}) in stimulated Raman loss modality. Definitely, since in our proposed microscope, the femtosecond laser sources used are compatible with other nonlinear microscopy techniques, it could be integrated with multimodal microscopy.

2. SRS microscope in C–H region

It is worth noting that SRS microscopes are not commercially available, so in order to take advantage of their peculiarities, the only option is the homemade implementation. In order to set up an SRS microscope, two crucial issues have to be addressed:

- **Implementation of a high-frequency modulation transfer method:** SRS signal measures the pump-induced amplification of the Stokes pulse, detecting a tiny change in the transmitted probe light of the order of about 10^{-4}. Therefore, laser intensity noise and shot noise can reduce the SRS signal. In a high-frequency modulation transfer method, an electro-optic modulator (EOM) is used to modulate the pump and the modulation, is transferred to the probe beam, and can be detected by a photodiode (PD), after blocking the pump beam with a stack of optical filters. The PD output is connected by a low-pass filter to a lock-in amplifier (LIA), which demodulates the measured signal. SRS technique requires the extraction of a small alternative current (AC) signal at the sub-microvolt level from a noisy environment. A LIA is essentially a band-pass amplifier with variable central frequency and bandwidth, which allows to obtain a significant improvement in signal to noise ratio (S/N), using a phase sensitive detection. If the modulation frequency is faster than the typical laser noise (e.g., 1 MHz), high sensitivity detection is achieved at the moderate laser power required for biological and medical imaging [39–42].

- **Realization of two-dimensional (2D) images:** To obtain 2D images which can be achieved through beam scanning with 2D galvo mirrors and by a sequential collection of pixels, which are acquired and quantized in intensity by a data acquisition chain. The scanning mirrors (SMs) require three TTL signals that are made available by the microscope controller connected to the scan head unit: pixel clock, line sync, and frame sync. A 2D image is obtained by the synchronization of the forward detection unit with two SMs, which raster the focal spot across an x-y plane. The synchronization is achieved by managing (i) the PCI card (NI PCIe 6363) through an in-house LabVIEW program, (ii) the electrical signal detected by LIA, and (iii) the digital signals

provided by the microscope scanning unit controller. All images with 512 × 512 pixels were analyzed with ImageJ software. The acquisition of a single image matrix takes 16 s. However, for a correct image acquisition, setting a number of parameters is required (e.g., pixel dimension and pixel dwell time). With the aim to preserve all information in an image, Nyquist's theorem must be followed during the sampling frequency, while to ensure the correct correspondence between spatial coordinates of pixels and measured SRS value in each pixel, the integration time of LIA have to be set equal or comparable to the pixel dwell time [43–46].

A fundamental procedure when carrying out SRS imaging is microscope alignment. The pulsed pump (Ti:Sa laser) and probe (synchronized OPO) lasers have to be carefully overlapped both in space and time at the image plane in order to generate a high SRS signal. Microscope alignments can be realized by three steps:

1. **Spatial overlap of two beams**. The initial step is the alignment of OPO and Ti:Sa lasers so that each beam arrives to the microscope. Then, we choose to consider the OPO as a reference beam. The Ti:Sa laser beam is spatially overlapped to OPO beam on a position-sensitive detector.

2. **Temporal overlap of two beams:** Considering that the pump and probe beams have slightly different beam paths inside the OPO housing, they show a time delay of about 5 ns at the OPO exit. Temporal overlap is usually obtained by a finely tuneable optical delay line. Usually, two techniques can be used to obtain the temporal overlap of two beams. The first can be obtained using a fast PD and oscilloscope, while the second is based on cross-optical correlator. In the case of the first technique, a rough overlap of two beams is obtained (uncertainty of 10 ps), whereas an accurate temporal overlap is obtained using a cross-correlator (resolution of 1 fs).

3. **Alignment of the two beams inside the microscope:** The sample is preliminary observed with white light to individuate the desired field of view (FOV). Then, laser beams, entering the microscope by a side port of microscope, are aligned to reach the PD mounted on the upstream. In order to optimize the FOV, the illumination, the focal position of microscope objectives, and checking if the two beams are spatially overlapped could be very useful to acquire transmission images (TI) for both Ti:Sa laser and OPO output.

The scanning microscope focuses the two laser beams into the sample by a microscope objective. After interaction with the sample, transmitted output pulses are collected by an upper objective. A PD and a LIA allow to measure the result of the SRS process occurring in the focal volume of the specimen after removing the pump pulses by a stack of optical filters. Our SRS microscope is shown in **Figure 2**. It is constructed by combining a femtosecond SRS spectroscopy setup with an inverted optical microscope (Eclipse TE-2000-E, Nikon) equipped with mirror scanning unit (C2, Nikon). The two pulsed laser sources are (i) a femtosecond Ti:Sa laser (Chameleon Ultra II), with a pulse duration of ~140 fs, a repetition rate of 80 MHz, and wavelengths of 680–1080 nm, and (ii) a femtosecond synchronized optical parametric oscillator (SOPO-Chameleon Compact OPO) pumped by a Ti:Sa laser. The pulse duration of SOPO output is ~200 fs. The repetition rate is 80 MHz, and the emission wavelength range is 1000–1600 nm. By combining the two laser systems, a minimum photon energy difference of 2500 cm^{-1} can be

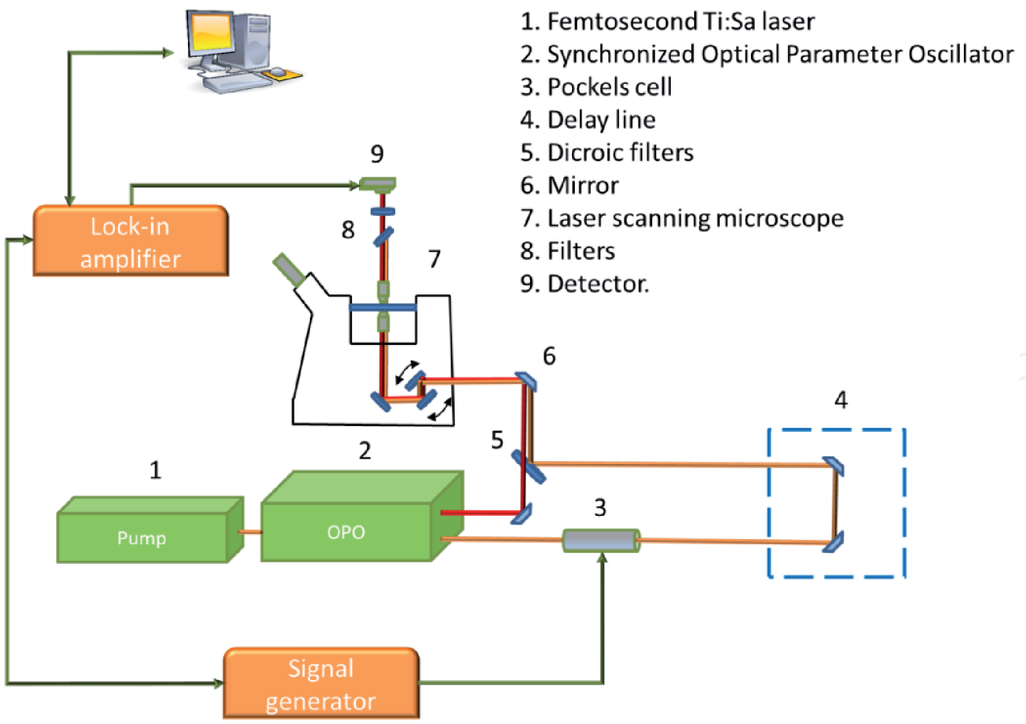

Figure 2.
Schematic experimental setup of the stimulated Raman scattering microscope.

obtained between the two beams. This means that only the high-frequency C-H region of Raman spectra (2800–3200 cm^{-1}) can be explored. Immediately following emission from the laser, the Ti:Sa laser pulses are modulated at a frequency of 4.5 MHz by an electro-optic modulator (EOM-CONOPTICS 350–160 KD*P) pulse selection system. Additionally, in order to obtain a temporal overlap between the two beams, a delay line (Newport MOD MILS200CC) was inserted between the Ti:Sa laser and the microscope. A dichroic mirror (Semrock FF875-Di01-125x36) spatially combines the collinear beams. The two beams were then focused into the specimen through a 60× multiphoton microscope objective (NA = 1.27). The output pulses are collected in transmission by a 40× high numerical aperture (NA = 1.25) multiphoton microscope objective. In order to remove the pump signal, a stack of optical filters was used, while the probe signal is measured by a photodetector (PD). The PD output is connected by a 50 Ω low-pass filter to a lock-in amplifier (LIA, SR844-200 MHz dual phase). The time constant in LIA was set to 100 μs with a slope of 18 dB/oct and a sensitivity of 10 μV [36, 37]. In order to collect information and to obtain a 2D image, the electrical signal coming out from the LIA is digitalized by PCI card (NI PCIe 6363), which manages and synchronizes the LIA and the scanning unit of microscope by an in-house developed LabVIEW program.

SRG images of a sample of polystyrene beads with a diameter of 3 μm were recorded. A strong SRG signal is observed from the polystyrene beads when the value of $\omega_L - \omega_S$ is matched to the C–H bond vibration at 3054 cm^{-1}. The obtained SRG and transmission images are shown in **Figure 3**. The pump signal was set at 810 nm, while the probe signal was set at 1073 nm. The focused power was less than 10 mW for both pump and probe beams. The transmission image was carried out with the single OPO laser at 1073 nm, and the transmitted beam intensity from the sample was measured by PD Thorlabs DET10N/M and directly acquired by the PCI card. The transmission image and the SRG image are given in **Figure 3(a)** and **(b)**, respectively.

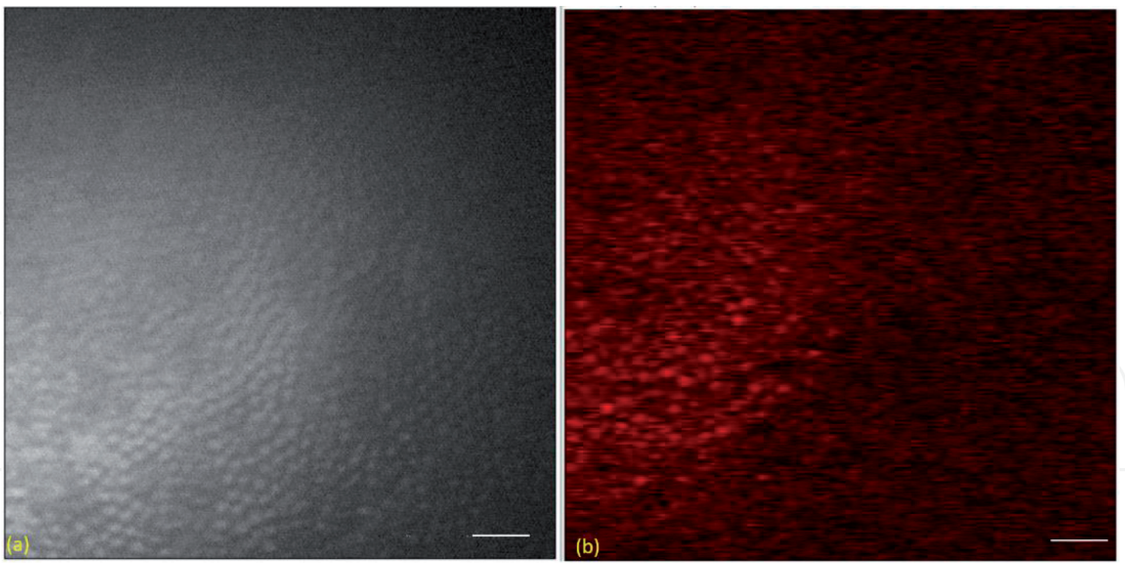

Figure 3.
(a) Transmission image and (b) SRG image of a polystyrene beads sample with a diameter of 3 μm. Scale bar corresponds to 25 μm.

2.1 Biological application in C–H region

Lipids are essential pillar for cells playing important roles for the maintenance of human health. Indeed, lipids act as signaling mediators, components of cellular membranes, and reservoirs for intracellular energy storage. Alterations in lipid metabolism are hallmarks of several human diseases, such as dyslipidemia, lipodystrophy, diabetes, obesity, atherosclerosis, heart diseases, and cancer.

The lipids are packed into specific intracellular organelles, termed lipid droplets, present in all cellular lines, but abundant in adipose and steroid-producing cells. LDs typically consist of neutral lipids in the form of triacylglycerols, cholesteryl esters, or retinyl esters encircled by a phospholipid monolayer with a surface made of numerous proteins that are involved in the regulation of lipid metabolism. Their sizes range from some tens of nanometer to tens of micrometer in diameter. LDs participate in a broad variety of physiological processes, such as lipid storage serving as fuels and/or such as biosynthetic precursors and signal transducers. Even though research is continuously growing in the relation between LDs and prominent diseases, a lot of fundamental questions are not yet resolved. In addition, new and unexpected connections with other cellular processes and pathologies are being found.

Traditionally LDs are imaged with fluorescence techniques of microscopy, using labelling fixed cells with neutral lipid specific dyes. However, lipids are smaller molecules than proteins and DNA, and their structures and functions are more susceptible to changes that might occur when adding fluorophores for imaging, introducing unwanted artifacts. Furthermore, their reluctant behavior to fluorescence dyes makes their identification and analysis difficult, especially for small LDs [47–60].

So far, most SRS applications have been aimed at label-free imaging of lipids in a variety of samples from artificial model systems to living cells and tissues. This prevalence is due to strong SRS signal for microscopy provided by LDs. Lipids are abundant in C–H_2 groups leading to a relatively isolated Raman peaks associated with C–H bond vibrational states at 2845 cm^{-1}, thus allowing to distinguish them from other chemical species. This peculiarity, together with the interest in the study of lipids and the possibility to image lipid structures, has encouraged SRS studies.

In the previous section, we have demonstrated the ability to acquire the images of the polystyrene beads in both transmission imaging and SRS modality of our system. In this section we are going to testify the biological application of SRS imaging technique. We have considered the distributions of LDs in 3T3-L1 cells at different stages of adipocyte differentiation: (i) 7 days and (ii) 15 days of growing time.

Adipocyte cells were grown on glass and fixed in PBS. To have a stable sample, the glass with the fixed cells is sandwiched between two coverslips. In order to obtain the image(s) of LDs inside adipocyte cells, the Raman shift of 2845 cm^{-1} associated with C–H_2 stretching mode has been investigated [40]. Hence, the Ti:Sa laser is set at 810 nm, and the wavelength of the OPO output is assigned to 1053 nm. After the power optimization of the laser beams (to avoid the thermal noises), the intensities of both lasers were set at 11 mW. Each acquired image is a single collection with 512 × 512 pixels. The acquisition time was 16 s. The LIA time constant was fixed to 100 μs with a slope of 16 dB/oct and a sensitivity of 10 μV.

Figure 4(a) shows the transmission image acquired image obtained with the OPO at wavelength of 1053 nm. The region of interest is first identified with this modality. **Figure 4(b)** shows the vibrational SRS contrast imaging. The bright regions indicate the individual lipid droplets. Small LDs are observable. The merge between the two images (a) and (b) is reported in **Figure 4(c)**. It highlights LD distribution inside the cells and its typical crown arrangement around the cell nucleus.

With the same procedure, we performed the analysis on a sample of adipocyte cells with 15 days of growing time. The results are shown in **Figure 5** for the transmission image obtained with OPO, SRS image, and the merge image.

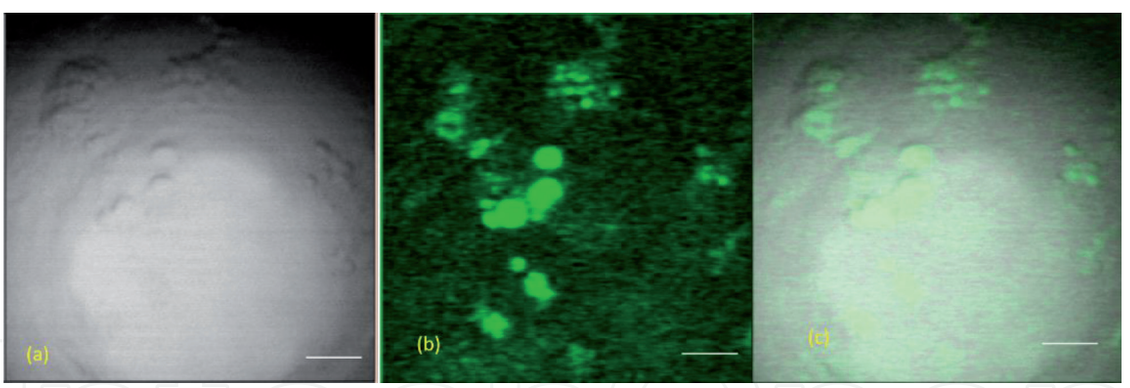

Figure 4.
Adipocyte cells at 7 days (D7): (a) transmission image by OPO, (b) SRS image of the sample, (c) merged image of transmission and SRS. Scale bar corresponds to 10 μm.

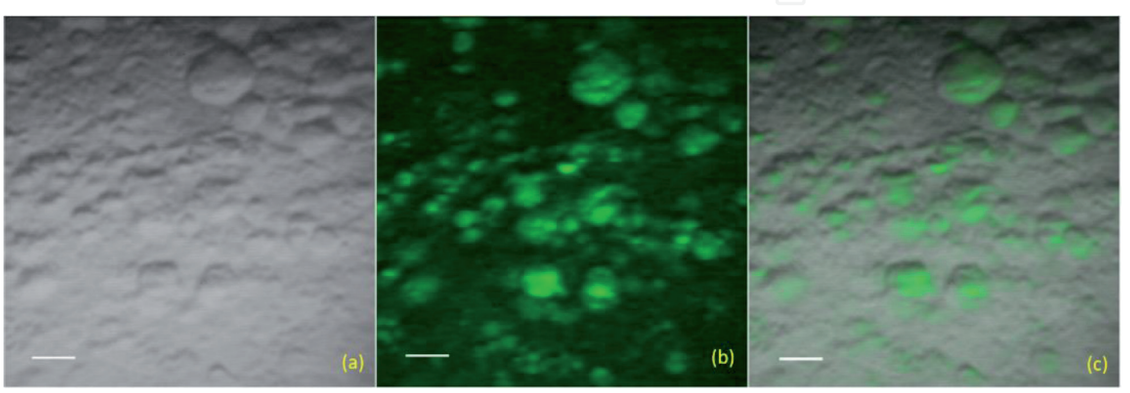

Figure 5.
Adipocyte cells at 15 days (D15) of growing time: (a) transmission image, (b) SRS image of the sample, and (c) merged image of absorption and SRS that indicates the LD distribution. Scale bar corresponds to 10 μm.

During our analysis in both the samples, we found that heterogeneity in LD size ranges from a few microns until 10 microns and beyond. Definitely, our findings indicate that SRS imaging is an alternative imaging tool when we cannot use fluorescence microscopy successfully.

3. Extension to the fingerprint region

The extension of the microscope to the silent region (<1800 cm^{-1}) and fingerprint region (1800–2800 cm^{-1}) is achieved by adding a SHG, cascading the OPO, and the SHG provides to double the OPO energy radiation. In our experimental setup, we used a flip mirror (FM) after the OPO exit to switch the Ti:Sa-OPO and Ti:Sa-SHG laser combinations. When the FM is inserted in the optical path, OPO radiation is coupled into SHG, so Ti:Sa-SHG laser combination becomes available, whereas when the FM is flipped, the OPO can go on undisturbed, and Ti:Sa-OPO laser combination becomes available (see **Figure 6**) [35].

Ti:Sa and OPO beams were spatially collinearly combined by a dichroic mirror (DM1) as described in the previous section. Ti:Sa-SHG beams were spatially collinearly combined by a dichroic mirror (DM2; Semrock FF735-Di0125x36), which is placed after DM1. Since DM2 is a high band-pass filter, whose transparence band starts at 735 nm, all wavelengths selected by the Ti:Sa-OPO laser combination are transmitted. Therefore, SRG acquisition in the Ti:Sa-OPO combination is not influenced by the presence of DM2.

Considering the Ti:Sa laser excitation with a wavelength range of 740–880 nm, the corresponding OPO emission range is 1000–1600 nm, while the SHG emission range is 500–800 nm. When the Ti:SA is used as pump at 830 nm, the largest range of Raman shift is obtained. Indeed, in this case all the region of Raman spectra can be covered (from 451 cm^{-1} to 3195 cm^{-1}) using the Ti:Sa-SHG laser combination.

The use of EOM in the implementation of SRS microscope leads to some drawbacks: increasing the cost of system, covering more space on the optical bench, and yielding unwanted electromagnetic interference. To avoid these disadvantages, save time for alignment, and increase flexibility of setup, the use of a single EOM with a fixed position on the bench is desirable. For these reasons, we implemented our SRS microscope with only one EOM. It is important to underline that the choice of laser source modulated by EOM has relevant consequences, because it settles the modalities SRL or SRG that can be utilized. We have chosen to use the EOM (350–160 KD*P CONOPTICS) for the intensity modulation of Ti:Sa laser pulses at a frequency *f* in the range of 1–30 MHz. For the Ti:Sa and OPO combination, only the SRG scheme can be thus implemented because the modulated laser beam energy is

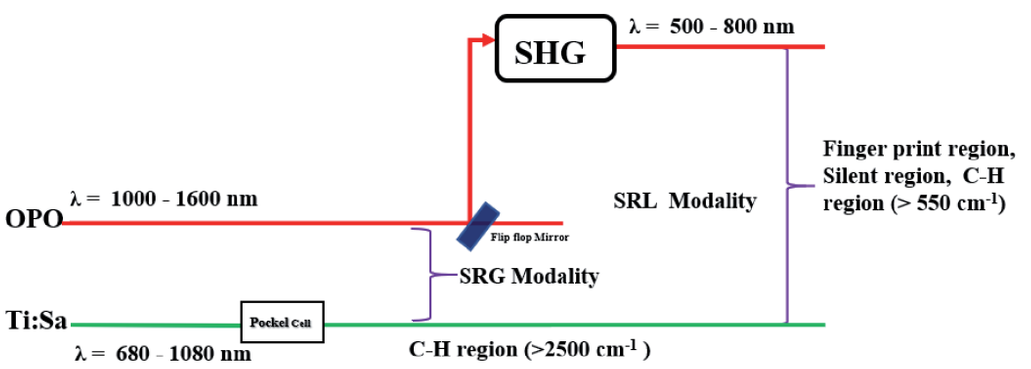

Figure 6.
Generation system with combination Ti:Sa-OPO (SRG modality) and Ti:Sa-SHG (SRL modality).

always greater than the other one. For the Ti:Sa-SHG combination, the SRL scheme can be implemented, since the modulated laser beam energy is always lower than the other one.

With the same scope to both reduce cost and save space, the use of a single delay line that allows coexistence between SRL and SRG optical circuitries is desirable. When the Ti:Sa-SHG laser configuration is used, the SHG only introduces an additional optical path with respect to Ti:Sa laser, with the delay time inside the SHG unchanged with respect to OPO. Therefore, in such configuration, temporal overlap between Ti:Sa and SHG laser pulses is achieved by a fixed shift movement of delay line with respect to the Ti:Sa-OPO overlap position. In our system, a single delay line with a fixed position on the bench is used, and the temporal overlap of each combination is achieved only by changing the direction of the delay line fixed shift movement, allowing a good flexibility (see **Figure** 7).

Again, in order to reduce cost and save space, a further important requirement is the use of a sole microscope for both optical circuits. In our setup, both laser combinations are then focalized and scanned on the sample. The output pulses are collected, as described in the previous section.

In particular, the collected radiations are incident onto a high band-pass optical filter (Dichroic filter FF875-Di01-25x36), whose transmission band starts at 875 nm, leading to two perpendicular optical paths. The OPO output is transmitted on the longitudinal path, while both Ti:Sa and SHG beams are reflected in the perpendicular path. Two photodiodes (PD1, PD2) positioned to the end of each path detect the unmodulated pulses (OPO beam for SRG modality and SHG beam for SRL modality), while the Ti:Sa modulated beam (pump pulses in SRG configuration and Stokes pulses in SRL configuration) is filtered. In order to enhance the acquisition efficiency, a Thorlabs detector (PD2; DET10N/M, InGaAs Detector) was used for SRG measurements, while a Thorlabs detector (PD1; DET10A/M, Si Detector) was used for SRL measurement. A stop line notch filter (Semrock NF03-808E-25) with band-pass of 788–828 nm is used to remove the Ti:Sa modulated beam. For SRL modality, a further filter (Semrock FF01–680/42–25) with band-pass 660–701 nm is added before photodiode to remove Ti:Sa residual pump beam. Finally, photodiode readout is demodulated by the same LIA introduced before to extract the modulation depth at the frequency *f*.

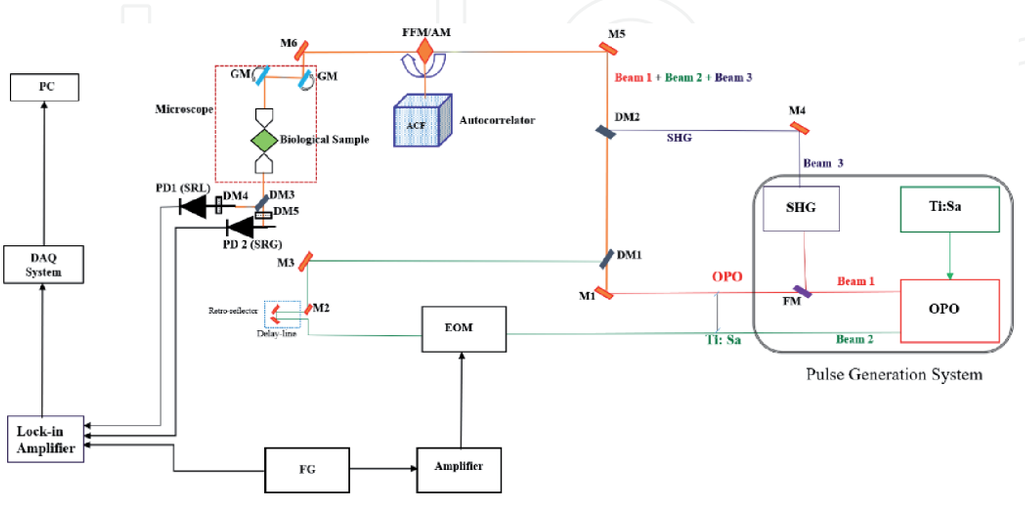

Figure 7.
Schematic layout of the f-SRS microscope. Ti:Sa, titanium-sapphire laser; OPO, optical parametric oscillator; SHG, second-harmonic generator; M1–M6, mirrors; FM, flip mirror; FFM/AM, flip flop mirror/autocorrelator mirror; ACF, autocorrelator function DM1, DM2, DM3, dichroic mirror; DM4, DM5, notch filters; EOM, electro-optic modulator; FG, function generator; GM, galvo mirror; PD1, PD2, photodiode; DAQ, data acquisition system; PC, personal computer.

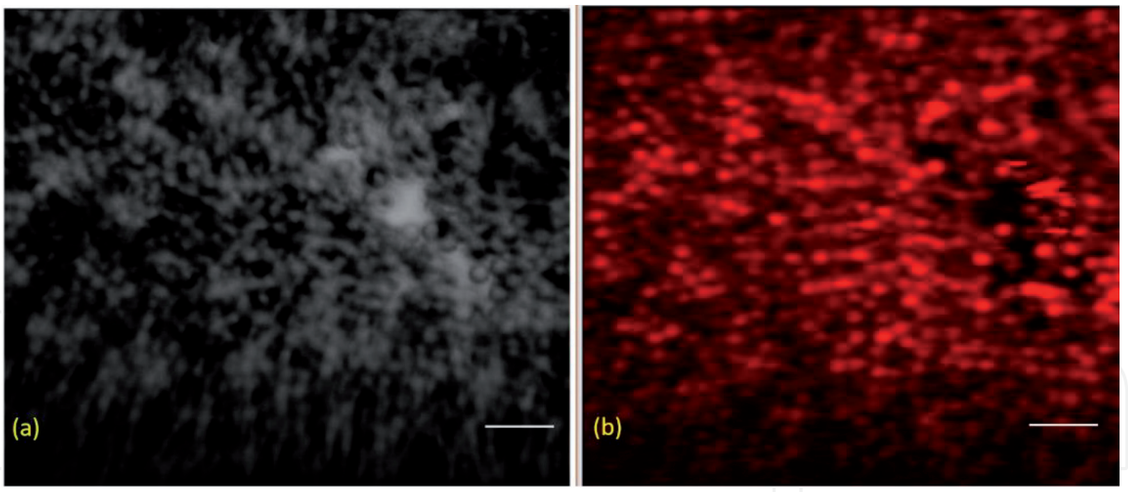

Figure 8.
(a) Transmission image and (b) SRL image of a polystyrene beads sample with a diameter of 3 μm. Scale bar corresponds to 25 μm.

To validate SRL imaging, the same PBS solution of polystyrene beads sample with diameter of 3 μm was used. The Raman shift was 3054 cm^{-1}, related to C–H bond. To record the image, the average focused power levels were 8 mW for pump beam at 650 nm generated by SHG unit and 10 mW for Stokes beam at 811 nm generated by Ti:Sa laser. The transmission image and the SRL image are shown in **Figure 8(a)** and **(b)**, respectively. In this case, the transmission image is obtained using a single beam at 650 nm. The transmitted beam intensity from the sample is measured by Thorlabs DET100A/M and directly acquired by the PCI card.

4. Conclusions

In this chapter, the design and the implementation of a nonlinear microscope based on stimulated Raman scattering is described. The presented microscope is equipped with three femtosecond laser sources: a titanium-sapphire laser, an optical parametric oscillator, and a second-harmonic generator (SHG) cascading the OPO. These three laser sources allow to cover all regions of Raman spectra by implementing two possible combinations. One consists in the use of Ti:Sa laser and OPO, which covers the C–H region or O–H region (>2800 cm^{-1}) in stimulated Raman gain (SRG) modality. Another with Ti:Sa laser and SHG covers not only the C–H region but also the fingerprint region (<1800 cm^{-1}) and the silent region (1800–2800 cm^{-1}) in stimulated Raman loss (SRL) modality. Therefore, our stimulated Raman scattering microscope allows the coexistence of SRG and SRL detection modes in a single microscopy setup and to acquire images of the same region in sequence without changing the optical components. Both SRL and SRG images of polystyrene beads are acquired by switching two combinations.

Finally, a biological case study in C–H region is reported, too. Our results confirmed that SRS imaging provides an advanced label-free approach to image and follow changes in lipid droplets potentially under physiological and pathological conditions.

Acknowledgements

The authors would like to thank Dr. G. Cozzi, a product specialist from Nikon Instruments, for his support in the SRS microscopy implementation and

Dr. M. Indolfi and Dr. V. Tufano (IMM-CNR) for their precious and constant technical assistance. The authors are also grateful to Angela Filograna and Carmen Valente of the Institute of Protein Biochemistry (CNR) for providing us with the adipocyte samples.

Conflict of interest

The authors declare that they have no competing financial interests.

Author details

Rajeev Ranjan[1,2*], Maria Antonietta Ferrara[1] and Luigi Sirleto[1]

1 National Research Council (CNR), Institute of Applied Sciences and Intelligent Systems, Napoli, Italy

2 CHT@Erzelli, Nanoscopy, Istituto Italiano Di Tecnologia, Genova, Italy

*Address all correspondence to: rajeev.ranjan@iit.it

References

[1] Streets AM, Li A, Chen T, Huang Y. Imaging without fluorescence: Nonlinear optical microscopy for quantitative cellular imaging. Analytical Chemistry. 2014;**86**:8506-8513. DOI: 10.1021/ac5013706

[2] Min W, Freudiger CW, Lu S, Xie XS. Coherent nonlinear optical imaging: Beyond fluorescence microscopy. Annual Review of Physical Chemistry. 2011;**62**:501-530. DOI: 10.1146/annurev.physchem.012809.103512

[3] Popp J, Kiefer W. Raman scattering, fundamentals. In: Meyers RA, editor. Encyclopedia of Analytical Chemistry. Wiley; 2000. pp. 13104-13142

[4] Freudiger CW, Min W, Saar BG, Lu S, Holtom GR, He C, et al. Label-free biomedical imaging with high sensitivity by stimulated Raman scattering microscopy. Science. 2008;**322**(5909):1857-1861. DOI: 10.1126/science.1165758

[5] Saar BG et al. Video-rate molecular imaging in vivo with stimulated Raman scattering. Science. 2010;**330**(6009):1368-1370

[6] Zumbusch A, Langbein A, Borri P. Nonlinear vibrational microscopy applied to lipid biology. Progress in Lipid Research. 2013;**52**(4):615-632. DOI: 10.1016/j.plipres.2013.07.003

[7] Alfonso-García A, Mittal R, Lee ES, Potma EO. Biological imaging with coherent Raman scattering microscopy: A tutorial. Journal of Biomedical Optics. 2014;**19**(7):071407. DOI: 10.1117/1.JBO.19.7.071407

[8] Zhang D, Wang P, Slipchenko MN, Cheng JX. Fast vibrational imaging of single cells and tissues by stimulated Raman scattering microscopy. Accounts of Chemical Research. 2014;**47**(8):2282-2290. DOI: 10.1021/ar400331q

[9] Cheng JX, Xie XS. Vibrational spectroscopic imaging of living systems: An emerging platform for biology and medicine. Science. 2015;**350**(6264):aaa8870. DOI: 10.1126/science.aaa8870

[10] Camp CH Jr, Cicerone MT. Chemically sensitive bioimaging with coherent Raman scattering. Nature Photonics. 2015;**9**(5):295-305. DOI: 10.1038/nphoton.2015.60

[11] Fu D. Quantitative chemical imaging with stimulated Raman scattering microscopy. Current Opinion in Chemical Biology. 2017;**39**:24-31. DOI: 10.1016/j.cbpa.2017.05.002

[12] Lee HJ, Cheng J-X. Imaging chemistry inside living cells by stimulated Raman scattering microscopy. Methods. 2017;**128**:119-128. DOI: 10.1016/j.ymeth.2017.07.020

[13] Mc Clung FJ, Hellwarth RW. Giant optical pulsations from ruby. Journal of Applied Physics. 1962;**33**:828-829. DOI: 10.1364/AO.1.S1.000103

[14] Shen YR, Bloembergen N. Theory of stimulated Brillouin and Raman scattering. Physics Review. 1965;**137**:A1787-A1805. DOI: 10.1103/PhysRev.137.A1787

[15] Garmire E, Pandarese F, Townes CH. Coherently driven molecular vibrations and light modulation. Physical Review Letters. 1963;**11**:160-163. DOI: 10.1103/PhysRevLett.11.160

[16] Sirleto L, Vergara A, Ferrara MA. Advances in stimulated Raman scattering in nanostructures. Advances in Optics and Photonics. 2017;**9**(1):169-217. DOI: 10.1364/AOP.9.000169

[17] Ferrara MA, Sirleto L. Stimulated Raman scattering in micro- and nanophotonics. In: Lembrikov BI, editor. Nonlinear Optics - Novel Results in Theory and Applications. Rijeka: IntechOpen; 2018. DOI: 10.5772/intechopen.80814

[18] Sirleto L, Ferrara MA, Nikitin T, Novikov S, Khriachtchev L. Giant Raman gain in silicon nanocrystals. Nature Communications. 2012;**N.3**:1-6. DOI: 10.1038/ncomms2188, article number: 1220

[19] Sirleto L, Ferrara MA, Vergara A. Toward an ideal nanomaterial for on-chip Raman laser. Journal of Nonlinear Optical Physics and Materials. 2017;**26**. DOI: 10.1142/S0218863517500394

[20] Wei L, Hu F, Chen Z, Shen Y, Zhang L, Min W. Live-cell bioorthogonal chemical imaging: Stimulated Raman scattering microscopy of vibrational probes. Accounts of Chemical Research. 2016;**49**(8):1494-1502

[21] Hu F, Lamprecht MR, Wei L, Morrison B, Min W. Bioorthogonal chemical imaging of metabolic activities in live mammalian hippocampal tissues with stimulated Raman scattering. Scientific Reports. 2016;**6**(1):39660

[22] Wei L, Hu F, Shen Y, Chen Z, Yu Y, Lin CC, et al. Live-cell imaging of alkyne-tagged small biomolecules by stimulated Raman scattering. Nature Methods. 2014;**11**(4):410-412. DOI: 10.1038/nmeth.2878

[23] Wei L, Shen Y, Xu F, Hu F, Harrington JK, Targoff KL, et al. Imaging complex protein metabolism in live organisms by stimulated Raman scattering microscopy with isotope labeling. ACS Chemical Biology. 2015;**10**(3):901-908. DOI: 10.1021/cb500787b

[24] Zhang D, Slipchenko MN, Cheng JX. Highly sensitive vibrational imaging by femtosecond pulse stimulated Raman loss. Journal of Physical Chemistry Letters. 2011;**2**(11):1248-1253. DOI: https://doi.org/10.1021/jz200516n

[25] Zhang C, Li J, Lan L, Cheng JX. Quantification of lipid metabolism in living cells through the dynamics of lipid Droplets measured by stimulated Raman Scattering Imaging. Analytical Chemistry. 2017;**89**(8):4502-4507. DOI: 10.1021/acs.analchem.6b04699

[26] Dou W, Zhang D, Jung Y, Cheng J-X, Umulis DM. Label-free imaging of lipid-droplet intracellular motion in early Drosophila embryos using femtosecond-stimulated Raman loss microscopy. Biophysical Journal. 2012;**102**(7):1666-1675. DOI: 10.1016/j.bpj.2012.01.057

[27] Zhang C, Huang K-C, Rajwa B, Li J, Yang S, Lin H, et al. Stimulated Raman scattering flow cytometry for label-free single-particle analysis. Optica. 2017;**4**(1):103. DOI: 10.1364/OPTICA.4.000103

[28] Lee HJ, Zhang W, Zhang D, Yang Y, Liu B, Barker EL, et al. Assessing cholesterol storage in live cells and *C. elegans* by stimulated Raman scattering imaging of phenyl-diyne cholesterol. Scientific Reports. 2015;**5**(1):7930. DOI: 10.1038/srep07930

[29] Li J, Cheng J-X. Direct visualization of De novo Lipogenesis in single living cells. Scientific Reports. 2015;**4**(1):6807. DOI: 10.1038/srep06807

[30] Hu C-R, Zhang D, Slipchenko MN, Cheng J-X, Hu B. Label-free real-time imaging of myelination in the *Xenopus laevis* tadpole by in vivo stimulated Raman scattering microscopy. Journal of Biomedical Optics. 2014;**19**(8):086005. DOI: 10.1117/1.JBO.19.8.086005

[31] Zipfel WR, Williams RM, Webb WW. Nonlinear magic: Multiphoton microscopy in the biosciences. Nature Biotechnology. 2003;**21**(11):1369-1377. DOI: 10.1038/nbt899

[32] Hoover EE, Squier JA. Advances in multiphoton microscopy technology. Nature Photonics. 2013;**7**(2):93-101. DOI: 10.1038/nphoton.2012.361

[33] D'Arco A, Brancati N, Ferrara MA, Indolfi M, Frucci M, Sirleto L. Subcellular chemical and morphological analysis by stimulated Raman scattering microscopy and image analysis techniques. Biomedical Optics Express. 2016;**7**(5):1853-1864. DOI: 10.1364/BOE.7.001853

[34] D'Arco A, Ferrara MA, Indolfi M, Tufano V, Sirleto L. Label-free imaging of small lipid droplets by femtosecond-stimulated Raman scattering microscopy. Journal of Nonlinear Optical Physics and Materials. 2017;**26**(4):1750052. DOI: 10.1142/S0218863517500527.Jnopm

[35] Ranjan R, D'arco A, Ferrara MA, Indolfi M, Larobina M, Sirleto L. Integration of stimulated Raman gain and stimulated Raman losses detection modes in a single nonlinear microscope. Optics Express. 2018;**26**(20):26317-26326. DOI: 10.1364/OE.26.026317

[36] Ranjan R, Indolfi M, Ferrara, MA, Sirleto L. Implementation of a nonlinear microscope based on stimulated Raman scattering. Journal of Visualized Experiments. 2019;(149):e59614. DOI: 10.3791/59614

[37] Ferrara MA, Filograna A, Ranjan R, Corda D, Valente C, Sirleto L. Three-dimensional label-free imaging throughout adipocyte differentiation by stimulated Raman microscopy. PLoS One. 2019;**14**(5):e0216811. DOI: 10.1371/journal.pone.0216811

[38] Ranjan R, Ferrara MA, Filograna A, Valente C, Sirleto L. Femtosecond stimulated Raman microscopy: Home-built realization and a case study of biological imaging. Journal of Instrumentation. 2019;**14**:P09008. DOI: 10.1088/1748-0221/14/09/P09008

[39] Heritage JP, Allara DL. Surface picosecond Raman gain spectra of a molecular monolayer. Chemical Physics Letters. 1980;**74**(3):507-510. DOI: 10.1016/0009-2614(80)85262-6

[40] Levine BF, Shank CV, Heritage JP. Surface vibrational spectroscopy using stimulated Raman scattering. IEEE Journal of Quantum Electronics. 1979;**15**:1418-1432. DOI: 10.1109/JQE.1979.1069939

[41] Ozeki Y, Dake F, Kajiyama S, Fukui K, Itoh K. Analysis and experimental assessment of the sensitivity of stimulated Raman scattering microscopy. Optics Express. 2009;**17**(5):3651. DOI: 10.1364/OE.17.003651

[42] Nandakumar P, Kovalev A, Volkmer A. Vibrational imaging based on stimulated Raman scattering microscopy. New Journal of Physics. 2009;**11**:033026-033035. DOI: 10.1088/1367-2630/11/3/033026

[43] Qiang W, Merchant FA, Castleman K. Microscope Image Processing. San Diego, United States: Elsevier/Academic Press; 2008

[44] Serra J. Image Analysis and Mathematical Morphology. Orlando, FL, United States: Academic Press, Inc; 1993

[45] Gonzalez R, Woods R. Digital Image Processing. Upper Saddle River, NJ, USA: Prentice-Hall, Inc.; 2006

[46] Broeke J, Mateos PJ, Pascau J. Image Processing with ImageJ. Birmingham: Packt Publ; 2015

[47] Suzuki M, Shinohara Y, Ohsaki Y, Fujimoto T. Lipid droplets: Size matters. Journal of Electron Microscopy. 2011;**60**(1):S101-S116

[48] Yang L, Ding Y, Chen Y, Zhang S, Huo C, Wang Y, et al. The proteomics of lipid droplets: Structure, dynamics, and functions of the organelle conserved from bacteria to humans. Journal of Lipid Research. 2012;**53**(7):1245-1253. DOI: 10.1194/jlr R024117

[49] Thiam AR, Farese RV, Walther TC. The biophysics and cell biology of lipid droplets. Nature Reviews. Molecular Cell Biology. 2013;**14**(12):775-786. DOI: 10.1038/nrm3699

[50] Tirinato L, Pagliari F, Limongi T, Marini M, Falqui A, Seco J, et al. An overview of lipid droplets in cancer and cancer stem cells. Stem Cells International. 2017:1656053. DOI: 10.1155/2017/1656053

[51] Kinkel DA, Fernyhough ME, Helterline DL, Vierck JL, Oberg KS, Vance TJ, et al. Oil red-O stains nonadipogenic cells: a precautionary note. Cytotechnology. 2004;**46**:49-56. DOI: 10.1007/s10616-004-3903-4

[52] Ohsaki Y, Shinohara Y, Suzuki M, Fujimoto T. A pitfall in using BODIPY dyes to label lipid droplets for fluorescence microscopy. Histochemistry and Cell Biology. 2010;**133**:477-480. DOI: 10.1007/s00418010-0678-x

[53] Rizzatti V et al. Lipid droplets characterization in adipocyte differentiated 3T3-L1 cells: Size and optical density distribution. European Journal of Histochemistry. 2013;**57**(3):159-162. DOI: 10.4081/ejh.2013.e24

[54] Alfonso Garcia A et al. D38-cholesterol as a Raman active probe for imaging intracellular cholesterol storage. Journal of Biomedical Optics. 2016;**21**(6), article number: 061003-1:8. DOI: 10.1117/1.JBO.21.6.061003

[55] Mukherjee S, Zha X, Tabas I, Maxfield FR. Cholesterol distribution in living cells: Fluorescence imaging using dehydroergosterol as a fluorescent cholesterol analog. Biophysical Journal. 1998;**75**(4):1915-1925. DOI: 10.1016/S0006-3495(98)77632-5

[56] Fukumoto S, Fujimoto T. Deformation of lipid droplets in fixed samples. Histochemistry and Cell Biology. 2002;**118**(5):423-428. DOI: 10.1007/s00418-002-0462-7

[57] Kinkel A et al. Oil red-O stains non-adipogenic cells: A precautionary note. Cytotechnology. 2004;**46**(1):49-56. DOI: 10.1007/s10616-004-3903-4

[58] Farese RV, Walther TC. Lipid droplets finally get a little R-E-S-P-E-C-T. Cell. 2009;**139**:855-886. DOI: 10.1016/j.cell.2009.11.005

[59] Straub BK, Herpel E, Singer S, Zimbelmann R, Breuhahn K, Macher-Goeppinger S, et al. Lipid droplet-associated PAT-proteins show frequent and differential expression in neoplastic steatogenesis. Modern Pathology. 2010;**23**:480-492. DOI: 10.1038/modpathol.2009.191

[60] Pol A, Gross SP, Parton RG. Review: biogenesis of the multifunctional lipid droplet: Lipids, proteins, and sites. The Journal of Cell Biology. 2014;**204**(5):635-646. DOI: 10.1083/jcb.201311051